

Estimating Franck-Condon factors using an NMR quantum processor

¹Sharad Joshi, ¹Abhishek Shukla, Hemant Katiyar, ²Anirban Hazra, and ¹T. S. Mahesh*

¹Department of Physics and NMR Research Center,

²Department of Chemistry,

Indian Institute of Science Education and Research,
Pune 411008, India

Interaction of molecules with light may lead to electronic transitions and simultaneous vibrational excitations. Franck-Condon factors (FCFs) play an important role in quantifying the intensities of such vibronic transitions occurring during molecular photo-excitations. In this article, we describe a general method for estimating FCFs using a quantum information processor. The method involves the application of a translation operator followed by the measurement of certain projections. We also illustrate the method by experimentally estimating FCFs with the help of a three-qubit NMR quantum information processor. We describe two methods for the measurement of projections - (i) using diagonal tomography and (ii) using Moussa protocol. The experimental results agree fairly well with the theory.

PACS numbers: 33.70.Ca, 33.20.Wr, 03.67.Ac, 82.56.Jn, 82.56.-b

Keywords: Franck-Condon principle, translation operator, density matrix tomography, ancilla qubit, Moussa protocol

I. INTRODUCTION

Electronic transitions in molecules are often associated with transitions in vibrational levels, and such combined transitions are known as vibronic transitions [1]. In a vibronic transition, the displacements of the nuclei, owing to their higher masses, occur at a much slower pace than the electronic rearrangements. This phenomenon is contained in the Franck-Condon principle, which states that the transition probability between two vibronic levels depends on the overlap between the respective vibrational wavefunctions [2]. Thus, in a vibronic transition, the intensities of the absorption or emission spectra are dictated by Franck-Condon factors (FCFs) which are the squared magnitudes of the overlaps of vibrational wavefunctions. Estimating FCFs is an important task in understanding absorption and fluorescence spectra and related phenomena such as photo-induced dissociations [3].

In this work, we estimate FCFs using a three-qubit Nuclear Magnetic Resonance (NMR) quantum processor [4, 5]. Long coherence times and precise control on spin-dynamics make NMR systems ideal testbeds for studying various aspects of quantum information and quantum physics [6]. For example, probability distributions of a particle in various potentials has recently been studied using a five-qubit NMR processor [7]. We describe an elegant method based on the iterative application of a translation operator to achieve an arbitrarily high spatial resolution of probability distributions.

Here we estimate FCFs corresponding to a pair of harmonic oscillators as a function of their relative displacements. An important step in this method is the measurement of certain projection operators. In this article we illustrate two different approaches for the measurement,

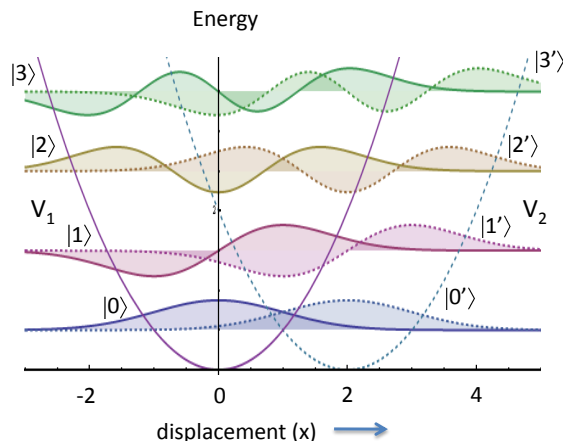


FIG. 1. A harmonic potential centred at the origin (V_1), a displaced harmonic potential centred at $x = 2$ and with $\Delta E = 0$ (V_2), and their corresponding wavefunctions. The unshifted eigenfunctions are labelled in the computational basis and the shifted eigenfunctions are indicated with primes.

namely (i) diagonal density matrix tomography and (ii) Moussa protocol.

In the following section we briefly describe the theory of FCFs and their estimation. The experimental results are described in section III and we conclude in section IV.

II. THEORY

A. Franck-Condon factors

In most of the vibronic transitions a molecule undergoes a transition from one electronic state to another,

* mahesh.ts@iiserpune.ac.in

both of which are described by smooth potential energy surfaces consisting of vibrational levels [2]. For low-lying vibrational levels, the potential energy surfaces along each vibrational degree of freedom can be approximated by simple harmonic potentials. Considering one vibrational degree of freedom, we model the electronic ground and excited vibrational levels as eigenstates of two harmonic potentials, V_1 and V_2 respectively (Figure 1). For simplicity, we choose the potentials $V_1 = x^2/2$ and $V_2 = (x - b)^2/2 + \Delta E$, which are identical up to an overall displacement b in position and/or in energy ΔE . Further, we have used unit mass and unit angular frequency, and therefore the kinetic energies $p^2/2$ will also be identical. Denoting $\mathbf{a} = (\mathbf{x} + i\mathbf{p})/\sqrt{2}$ and $\mathbf{a}^\dagger = (\mathbf{x} - i\mathbf{p})/\sqrt{2}$ respectively as the annihilation and creation operators, we choose the eigenstates $\{|n\rangle\}$ of the number operator $\mathbf{N} = \mathbf{a}^\dagger\mathbf{a}$ as our computational basis [8]. Thus the vibrational Hamiltonians for the two electronic states are

$$\begin{aligned}\mathcal{H}_1 &= \mathbf{p}^2/2 + \mathbf{x}^2/2 \\ &= \mathbf{a}^\dagger\mathbf{a} + 1/2 \quad \text{and,} \\ \mathcal{H}_2 &= \mathbf{p}^2/2 + (\mathbf{x} - b)^2/2 + \Delta E \\ &= (\mathbf{p}^2/2 + \mathbf{x}^2/2) + b^2/2 - \mathbf{x}b + \Delta E \\ &= \mathbf{a}^\dagger\mathbf{a} + 1/2 + b^2/2 - (\mathbf{a} + \mathbf{a}^\dagger)b/\sqrt{2} + \Delta E, \quad (1)\end{aligned}$$

where the reduced Planck's constant \hbar is set to unity. A general vibronic excitation constitutes a transition from a vibrational level $|m\rangle$ of the electronic ground state to a vibrational level $|n'\rangle$ of the electronic excited state. For each vibronic transition $|m\rangle \rightarrow |n'\rangle$, Franck-Condon principle assigns the probability,

$$W_{m,n'} \propto f_{m,n'}(b), \quad (2)$$

where

$$\begin{aligned}f_{m,n'}(b) &= |\langle m|n'\rangle|^2 \\ &= \left| \int_{-\infty}^{\infty} \psi_m^*(x)\psi_{n'}(x,b)dx \right|^2, \quad (3)\end{aligned}$$

are known as FCFs [2]. Here $\psi_m(x)$ and $\psi_{n'}(x,b)$ are the position wave-functions corresponding to the states $|m\rangle$ and $|n'\rangle$ respectively. Since we have chosen identical potentials with unit angular frequencies and unit masses, FCFs depend only on the displacement b . The separation in energy ΔE only shifts the eigenvalue corresponding to $|n'\rangle$ and does not affect the FCFs, and hence ΔE is set to zero. Theoretical FCFs corresponding to lowest four levels of harmonic potentials V_1 and V_2 are tabulated below.

B. Estimation of FCFs

Estimation of FCF, $f_{m,n'}$, is equivalent to measurement of expectation value of the projection $P_m = |m\rangle\langle m|$

$f_{0,0'}$	$e^{-b^2/2}$
$f_{0,1'}$	$e^{-b^2/2} b^2/2$
$f_{0,2'}$	$e^{-b^2/2} b^4/8$
$f_{0,3'}$	$e^{-b^2/2} b^6/48$
$f_{1,1'}$	$e^{-b^2/2} (b^2 - 2)^2/4$
$f_{1,2'}$	$e^{-b^2/2} (b^3 - 4b)^2/16$
$f_{1,3'}$	$e^{-b^2/2} (b^4 - 6b^2)^2/96$
$f_{2,2'}$	$e^{-b^2/2} (b^4 - 8b^2 + 8)^2/64$
$f_{2,3'}$	$e^{-b^2/2} (b^5 - 12b^3 + 24b)^2/384$
$f_{3,3'}$	$e^{-b^2/2} (b^6 - 18b^4 + 72b^2 - 48)^2/2304$

TABLE I. Analytical forms of FCFs as a function of displacement b for a pair of infinite-level identical harmonic oscillators.

after preparing the system in excited state $|n'\rangle$ since,

$$\begin{aligned}f_{m,n'} &= \langle n'|m\rangle\langle m|n'\rangle \\ &= \langle P_m \rangle_{n'}. \quad (4)\end{aligned}$$

FCFs can also be obtained, as described in the next section, by extracting the diagonal elements of the density matrix after preparing the state $|n'\rangle\langle n'|$.

Quantum simulation of a single harmonic potential has earlier been carried out by Cory and co-workers [9]. Here the vibrational levels of the electronic ground state are encoded onto the spin states such that $|0\rangle = |000\rangle$, $|1\rangle = |001\rangle$, $|2\rangle = |010\rangle$, $|3\rangle = |011\rangle$, and so on. Thus the preparation of vibrational level $|n\rangle$ of the electronic ground state is equivalent to preparing a specific spin state and can be achieved by standard methods as explained in the next section.

The preparation of excited state $|n'\rangle$ can be achieved by first initializing the system in the corresponding state $|n\rangle$ of the electronic ground state and translating it in position from origin ($x = 0$) to the point $x = b$. This translation can be achieved by the unitary operator

$$U_T(b) = e^{-i\mathbf{p}b}. \quad (5)$$

Discrete translations up to $b_0 \geq 0$ can be achieved by repetitively applying the operator $U_T(b_0/N)$ such that $U_T(b_0k/N) = [U_T(b_0/N)]^k$, where $k \leq N$ are non-negative integers. In the following we describe two experimental techniques to measure FCFs, one based on direct measurement of projection operators using diagonal density matrix tomography and the other based on Moussa protocol.

III. EXPERIMENTS

We have chosen the three spin-1/2 ^{19}F nuclei of iodotri-fluoroethylene ($\text{C}_2\text{F}_3\text{I}$) dissolved in acetone- D_6 as our three-qubit NMR quantum processor. All the experiments are carried out on a 500 MHz Bruker NMR spectrometer at an ambient temperature of 300 K. The molecular structure and the Hamiltonian parameters of this

system are given in Figure 2. In the following we describe two experimental methods for estimating FCFs.

A. Using diagonal density matrix tomography

The three-spin system C_2F_3I provides us with a 3-qubit quantum register which can be used to encode the lowest eight levels of a harmonic oscillator. To determine all FCFs corresponding to the lowest four levels, we carry out a set of four experiments each with a different initial state $\rho_{ini} = |n\rangle\langle n| \in \{|000\rangle, |001\rangle, |010\rangle, |011\rangle\}$ encoding a particular vibrational level of the electronic ground state. As is customary in NMR quantum information studies, each pure state is mimicked by preparing a corresponding pseudopure state which in turn is prepared by standard methods [10, 11].

As explained earlier, FCF $f_{m,n'}(b_0k/N) = \rho'_m = \langle m|\rho'|m\rangle$ is a diagonal element of the translated state $\rho' = U_T(b_0k/N)|n\rangle\langle n|U_T^\dagger(b_0k/N)$. In our experiments we have used $b_0 = 3$, $N = 11$, and integer $k \in [0, 11]$. The complete translation operator was realized using amplitude and phase modulated radio frequency pulses. These pulses were designed via GRADIENT ASCENT PULSE ENGINEERING (GRAPE) technique [12] and had average Hilbert-Schmidt fidelities above 0.99 over a spatial RF inhomogeneity in the range 90% to 110% of the nominal field.

The diagonal density matrix tomography involves destroying all the off-diagonal elements of ρ' using a pulsed-field-gradient (PFG) followed by linear detection using a small flip-angle (6 degree) y-pulse. The detection pulse mixes the diagonal elements ρ'_m into observable coherences which appear as various resolved transitions in the NMR signal. The real part r_j of j th transition normalized w.r.t. the reference (corresponding to equilibrium density matrix followed by the linear detection) constitutes a linear combination $r_j = \sum_m M_{j,m}\rho'_m$, where the coefficients $M_{j,m}$ form a 13×8 dimensional constraint matrix [11]. The diagonal elements ρ'_m can be extracted by solving the overdetermined set of linear equations [11].

The experimental values of all FCFs as a function of b

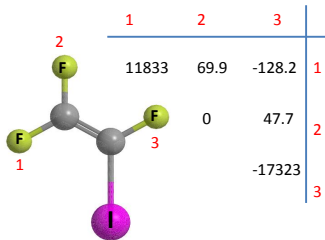


FIG. 2. Molecular structure of iodotrifluoroethylene and its Hamiltonian parameters. The diagonal elements represent relative resonance frequencies and the off-diagonal elements represent the strengths of scalar (J) couplings.

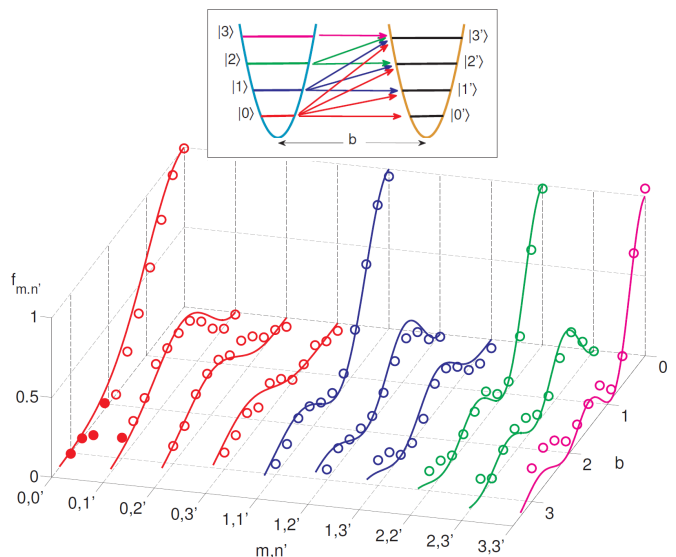


FIG. 3. Experimental FCFs (circles) corresponding to lowest four-levels of Harmonic oscillators (shown in inset) measured using diagonal density matrix tomography of 3-qubits. Analytical forms of FCFs (solid-line) for infinite-level potentials (Table I) are also plotted for comparison. All the FCFs are plotted versus displacement b . Filled circles indicate the FCFs which are entirely due to the overlap of tunnelling amplitudes.

for the lowest four levels of a pair of Harmonic oscillator are shown by circles in Fig. 3. The theoretical curves corresponding to infinite-level harmonic oscillators, are also shown for comparison. Since the FCFs are symmetric w.r.t. the exchange of subscripts, it can be noted that $f_{m,n'} = f_{n,m'}$. While there is a good agreement between the theoretical and experimental data, the errors are mainly due to imperfections in preparation of pseudopure states, imperfections in implementing the translation operators, and decoherence. The filled circles in Fig. 3 correspond to the overlap between the wavefunctions beyond the classical turning points, i.e., $b \geq 2$ for $f_{0,0'}$ and $b \geq 1 + \sqrt{3}$ for $f_{0,1'}$. Thus the non-zero values of FCFs at these points provide a direct way of experimental observation of quantum tunnelling.

B. Using Moussa protocol

As described in eqn. 4, estimating FCFs is equivalent to measurement of certain projections. An existing method, known as Moussa protocol [13], achieves the measurement of any unitary observable with the help of an ancilla qubit. The circuit implementation of Moussa protocol is illustrated in Figure 4a. It involves an ancilla qubit initialized in state $|+\rangle$ and the system is initialized in any desired state ρ . In order to measure the expectation value of a unitary observable S , we need to apply the operator on the system controlled by ancilla as shown in

Figure 4a. Then we obtain $\langle S \rangle$ by directly measuring σ_x operator on the ancilla [13], i.e.,

$$\langle S \rangle_\rho = \langle \sigma_x \rangle_{\text{an}}. \quad (6)$$

Here we extend this protocol to extract expectation values of a projection operator which can then be used to measure any general observable.

Let P be a projection operator, with $P^n = P$, for any positive integer n . Consider a unitary operator $S = \exp(iP\theta)$ with a chosen angle θ . Consider the circuit shown in Figure 4b. It can be shown that the expectations of ancilla are related to the S by [11]

$$\langle \sigma_x \rangle_{\text{an}} = \langle S + S^\dagger \rangle_\rho / 2, \quad \text{and} \quad \langle i\sigma_y \rangle_{\text{an}} = S - S^\dagger / 2,$$

so that

$$\langle \sigma_x \rangle_{\text{an}} + i\langle \sigma_y \rangle_{\text{an}} = \langle S \rangle_\rho = \langle e^{iP\theta} \rangle_\rho = 1 + \langle P \rangle_\rho (e^{i\theta} - 1),$$

and hence

$$\langle P \rangle_\rho = \frac{1 - \langle \sigma_x \rangle_{\text{an}}}{1 - \cos \theta}. \quad (7)$$

Taking $\theta = \pi$, we obtain $\langle P \rangle_\rho = (1 - \langle \sigma_x \rangle_{\text{an}}) / 2$.

In our experiments, we have selected F_1 qubit (see Figure 2) as the ancilla and the other two qubits for representing the lowest four levels of the Harmonic oscillator. As explained in the previous section, we first prepare the system in one of the four levels of the electronic ground state and translate it in position towards the corresponding excited state. Instead of initializing the system into a single level, we utilize the ‘Pair Of Pseudopure States’ (POPS) method [14] which prepares the system into a traceless pseudopure mixture of two levels $\rho_{j,k} = |j\rangle\langle j| - |k\rangle\langle k|$, where $j, k (\neq j) \in \{00, 01, 10, 11\}$ [11]. After applying the translation operator, we obtain the corresponding excited states $\rho'_{j,k} = |j'\rangle\langle j'| - |k'\rangle\langle k'|$. In our experiments, we have selected the projection operator $P_{00} = |00\rangle\langle 00|$ as our observable. This way, we determine the overlap between the level $|00\rangle$ of the electronic ground state with $|n'(b)\rangle$ of the electronic excited state, and obtain the FCFs $f_{00,k'}$.

The complete circuit with initialization and extended

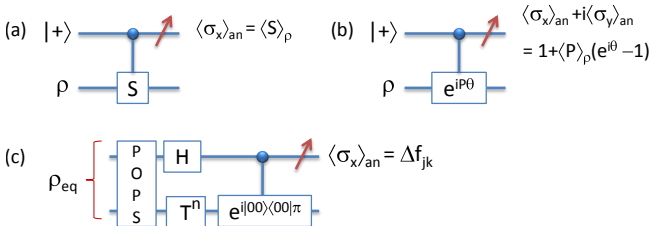


FIG. 4. Circuits for Moussa protocol (a), its extension (b), and the overall circuit for estimating FCFs. In all the cases the top qubit corresponds to ancilla and the remaining are system qubits. In (b) P is a projection observable.

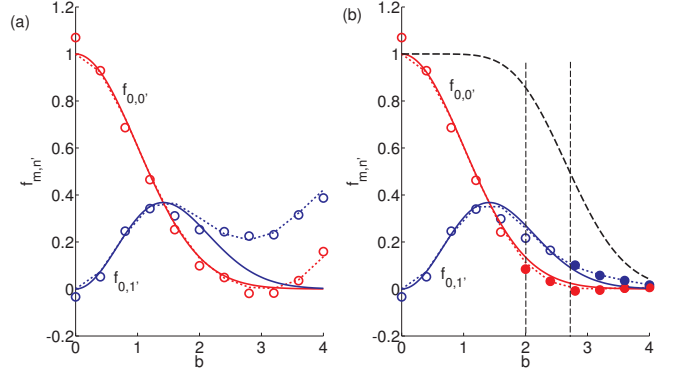


FIG. 5. Experimental FCFs (circles) corresponding to 4-level harmonic oscillators (encoded by two qubits) versus the displacement b obtained using Moussa protocol. The simulated FCFs (dotted lines) for the 4-level system and analytical FCFs (smooth lines) for infinite-level system (Table I) are also shown for comparison. The dashed curve at the top of (b) corresponds to the normalization used. The thin vertical dashed lines at $b = 2$, $1 + \sqrt{3}$ mark the beginning of classically forbidden regions for $f_{0,0'}$, $f_{0,1'}$ respectively.

Moussa protocol is shown in Figure 4c. Here the first qubit is the ancilla and the other two qubits form the system. We first applied the translation operator $U_T(b_0 k/N)$ after preparing the initial state $|+\rangle\langle +| \otimes \rho_{jk}$. In these experiments b_0 was set to 4 and N to 11. Again, the complete translation operator was realized using amplitude and phase modulated radio frequency pulses having fidelities over 0.995. Then the operator $\exp(iP_{00}\pi)$ on the system qubits controlled by the ancilla qubit was applied. The GRAPE pulse of this operator had an average fidelity of 0.989 over the similar RF inhomogeneity range. Finally the real part of the ancilla signal that is proportional to $\langle \sigma_x \rangle_{\text{an}}$ is measured by integrating the ancilla transitions. Thus after each preparation $\rho'_{j,k}$ we can extract the difference of FCFs $\Delta f_{j,k} = f_{00,j'} - f_{00,k'}$. In order to determine all individual FCFs of the form $f_{00,k'}$, we perform four different experiments and measure $\Delta f_{00,01'}$, $\Delta f_{00,10'}$, $\Delta f_{01,11'}$, and $\Delta f_{10,11'}$, and solve the four linear equations with the help of an additional constraint given by the normalization condition $\sum_j f_{00,j'} = F$.

The results of the experiment with $F = 1$ and for various values of $b \in [0, 4]$ are shown in Figures 5a. The experimental data points are shown by symbols. To understand the systematic errors in the experimental data, we have simulated FCF values using lowest four levels of the computational basis. In Figures 5 The simulated curves are shown by dotted lines and the expected FCF curves for infinite level systems are shown by smooth lines. Here a good agreement between the experimental results and the simulated curves can be observed. However, as can be readily seen, the observed FCFs gradually deviate away from the infinite case with increasing values of b . The deviation between the finite and infinite FCFs is due to

the effect of truncation in the basis-set, and can be minimized by increasing the number of system qubits [11].

If one has the prior information on the normalization condition F , it is possible to get better agreement with the infinite case. This is illustrated in Figures 5b. The total probability for the first four levels in the infinite-level case varies with b as $\sum_j f_{00,j} = [1 + b^2/2 + b^4/8 + b^6/48] e^{-b^2/2}$ and is shown by thin-dashed lines at the top of Figure 5b. The experimental results with this normalization are shown by symbols. With this normalization, the FCFs show considerably good agreement with the infinite-level case. Again FCFs in classically forbidden regions are shown by filled circles in 5b.

IV. CONCLUSIONS

We formulated a general procedure for estimating Franck-Condon Factors (FCFs) in a quantum informa-

tion processor. First we noted that an excited state can be prepared by spatially translating the corresponding ground state. Secondly, we observed that estimation of FCFs is equivalent to the measurement of certain projection operators on a set of qubits encoding the excited state of the system. We described two techniques of extracting the expectation values: one based on diagonal tomography and the other using an extended Moussa protocol. We illustrated both of these techniques using a three qubit NMR quantum simulator and compared the results with the simulated curves for finite and infinite level systems. We demonstrated that even with only three/two qubits encoding the system, the FCFs corresponding to the lowest four/two levels still matched fairly well with the infinite-level theory. In general, if we have an arbitrary potential for the excited state, then it may still be possible to prepare the final state using adiabatic evolutions.

-
- [1] G. Herzberg, *Spectra of diatomic molecules*, Vol. 1 (van Nostrand, 1950).
 - [2] W. Demtroder, Heidelberg, Springer-Verlag Berlin Heidelberg, 2006. 571 (2006).
 - [3] W. D. Bowers, S. S. Delbert, R. L. Hunter, and R. T. McIver Jr, *Journal of the American Chemical Society* **106**, 7288 (1984).
 - [4] D. G. Cory, R. Laflamme, E. Knill, L. Viola, T. Havel, N. Boulant, G. Boutis, E. Fortunato, S. Lloyd, R. Martinez, *et al.*, *Fortschritte der Physik* **48**, 875 (2000).
 - [5] D. Suter and T. S. Mahesh, *The Journal of chemical physics* **128**, 052206 (2008).
 - [6] I. Oliveira, R. Sarthour Jr, T. Bonagamba, E. Azevedo, and J. C. Freitas, *NMR quantum information processing* (Elsevier, 2011).
 - [7] R. Shankar, S. S. Hegde, and T. S. Mahesh, *Physics Letters A* **378**, 10 (2014).
 - [8] R. Shankar, *Principles of quantum mechanics*, Vol. 233 (Plenum Press New York, 1994).
 - [9] S. Somaroo, C. Tseng, T. Havel, R. Laflamme, and D. G. Cory, arXiv preprint quant-ph/9905045 (1999).
 - [10] D. G. Cory, M. D. Price, and T. F. Havel, *Physica D* **120**, 82 (1998).
 - [11] see supplementary material, .
 - [12] N. Khaneja, T. Reiss, C. Kehlet, T. Schulte-Herbrüggen, and S. J. Glaser, *Journal of Magnetic Resonance* **172**, 296 (2005).
 - [13] O. Moussa, C. A. Ryan, D. G. Cory, and R. Laflamme, *Physical review letters* **104**, 160501 (2010).
 - [14] B. Fung, *Physical Review A* **63**, 022304 (2001).

SUPPLEMENTARY MATERIAL

A. Finding expectation value of a general unitary operator using Moussa protocol

Consider a general unitary operator U . To determine its expectation value we prepare the system in any desired state ρ , ancilla in state $|+\rangle$, and apply the Moussa protocol as shown in Fig. 2. The state of the combined system evolves under the controlled- U operation as

$$|+\rangle\langle+| \otimes \rho \xrightarrow{U} \frac{1}{2} \{ |0\rangle\langle 0| \otimes \rho + |0\rangle\langle 1| \otimes \rho U^\dagger + |1\rangle\langle 0| \otimes U\rho + |1\rangle\langle 1| \otimes U\rho U^\dagger \}. \quad (8)$$

After tracing out system, the ancilla becomes

$$\frac{1}{2} \{ |0\rangle\langle 0| + |0\rangle\langle 1| \langle U^\dagger \rangle + |1\rangle\langle 0| \langle U \rangle + |1\rangle\langle 1| \} = \begin{bmatrix} 1 & \langle U^\dagger \rangle \\ \langle U \rangle & 1 \end{bmatrix}. \quad (9)$$

In an NMR signal obtained with a quadrature detection, the real and imaginary parts correspond to the expectation values of σ_x and σ_y observables respectively [Ref]. Thus the real and imaginary parts of the ancilla signal are proportional to $\langle \sigma_x \rangle = \langle \frac{U+U^\dagger}{2} \rangle$ and $\langle i\sigma_y \rangle = \langle \frac{U-U^\dagger}{2} \rangle$, from which the expectation value $\langle U \rangle = \langle \sigma_x \rangle + i\langle \sigma_y \rangle$ can be extracted.

B. Extracting expectation value of a Hermitian operator compatible with a pure-state

The circuit for this measurement is shown in Figure 3. Given the Hermitian operator A to be compatible with a pure state ρ , we can simultaneously diagonalize both of these using a similarity transformation U_s , i.e., $A_d = U_s^\dagger A U_s$, $\rho_d = U_s^\dagger \rho U_s$ are diagonal, and therefore $\langle A_d \rangle_{\rho_d} = \langle A \rangle_\rho$. As shown above, the complex ancilla signal corresponds to $\langle \sigma_x \rangle_{\text{an}} + i \langle \sigma_y \rangle_{\text{an}} = \langle e^{iA_d \theta} \rangle_{\rho_d}$. In the following we prove that $\langle e^{iA_d \theta} \rangle_{\rho_d} = e^{i \langle A_d \rangle_{\rho_d} \theta}$. Since the system is in a pure state, we can write $\rho_d = |n\rangle\langle n|$ and $(\rho_d)_{ij} = \delta_{in} \delta_{jn}$. Now consider,

$$\begin{aligned} \langle A_d^k \rangle_{\rho_d} &= \text{Tr} [\rho_d A_d^k] \\ &= \sum_i (\rho_d A_d^k)_{ii} \\ &= \sum_{i j_1 j_2 \dots j_k} \delta_{in} \delta_{j_1 n} (A_d)_{j_1 j_2} \dots (A_d)_{j_k i} \\ &= (A_d)_{nn}^k, \quad \text{since } A_d \text{ is diagonal.} \end{aligned} \quad (10)$$

For $k = 1$, we have $\langle A_d \rangle_{\rho_d} = (A_d)_{nn}$, and therefore $\langle A_d^k \rangle_{\rho_d} = \langle A_d \rangle_{\rho_d}^k$, which implies, $\langle e^{iA_d \theta} \rangle_{\rho_d} = e^{i \langle A_d \rangle_{\rho_d} \theta}$. Since $\langle A_d \rangle_{\rho_d} = \langle A \rangle_\rho$, we have $\langle \sigma_x \rangle_{\text{an}} + i \langle \sigma_y \rangle_{\text{an}} = e^{i \langle A \rangle_\rho \theta}$.

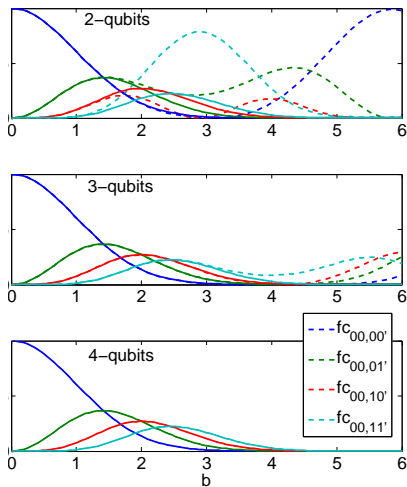


FIG. 6. Numerical simulation of FCFs to show the effect of truncation of basis (i.e., finite levels of the potentials). 4-basis states (top-panel), 8-basis states (middle-panel), and 16-basis states (bottom-panel) are used to simulate FCFs.

Hermitian operator compatible with a pure-state: Let the system be in a pure state ρ and A be a Hermitian operator compatible with ρ , i.e., they have a common eigenbasis. We can transform ρ into its eigenbasis using a similarity transformation U_s , such that $\rho = U_s \rho_d U_s^\dagger$, $A = U_s A_d U_s^\dagger$, where ρ_d and A_d are diagonal. Again we can perform the Moussa protocol (Figure 4c) by applying the unitary $S = \exp(iA_d \theta)$ controlled by ancilla, and we obtain [11],

$$\langle \sigma_x \rangle_{\text{an}} + i \langle \sigma_y \rangle_{\text{an}} = e^{i \langle A \rangle_\rho \theta}. \quad (11)$$

The expectation $\langle A \rangle_\rho$ can be extracted by knowing the rotation angle θ .

Numerical simulations on the effect of finite-basis is illustrated in Fig. 6.

Finally to demonstrate the robustness of these methods, calculated FCFs by adding random numbers (between $-\eta$ and η) to simulated the NMR intensities (see Fig. 7). The average standard deviation $\langle \sigma_\epsilon \rangle$ of FCFs as a function of noise amplitude η is shown in Figure 7. It can be observed that $\langle \sigma_\epsilon \rangle < 0.2$ for both the methods even at $\eta = 1$, indicating the robustness of the methods.

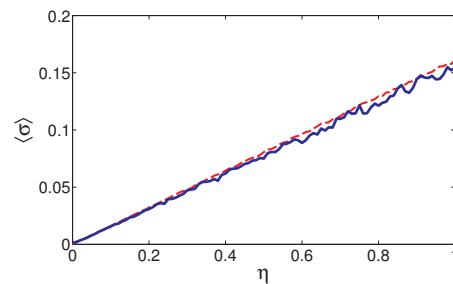


FIG. 7. Average standard deviation of simulated FCFs as a function of noise amplitude η . The blue solid-line corresponds to the diagonal-tomography method and the red dashed-line corresponds to Moussa protocol.